

A Mott insulator induced near iron pnictide superconductors

Yu Song,¹ Zahra Yamani,² Chongde Cao,^{1,3} Yu Li,¹ Chenglin Zhang,¹ Justin Chen,¹ Qingzhen Huang,⁴ Hui Wu,^{4,5} Jing Tao,⁶ Yimei Zhu,⁶ Wei Tian,⁷ Songxue Chi,⁷ Rong Yu,⁸ Andriy H. Nevidomskyy,¹ Emilia Morosan,¹ Qimiao Si,¹ and Pengcheng Dai¹

¹*Department of Physics and Astronomy, Rice University, Houston, Texas 77005, USA*

²*Canadian Neutron Beam Centre, Chalk River Laboratories, Chalk River, Ontario K0J 1J0, Canada*

³*Department of Applied Physics, Northwestern Polytechnical University, Xian 710072, China*

⁴*NIST Center for Neutron Research, National Institute of Standards and Technology, Gaithersburg, Maryland 20899, USA*

⁵*Department of Materials Science and Engineering,*

University of Maryland, College Park, MD 20742-2115, USA

⁶*Condensed Matter Physics and Materials Science Department,*

Brookhaven National National Laboratory, Upton, New York 11973, USA

⁷*Quantum Condensed Matter Division, Oak Ridge National Laboratory, Oak Ridge, Tennessee 37831, USA*

⁸*Department of Physics, Renmin University of China, Beijing, 100872, China*

Iron-based superconductivity develops out of a bad-metal state, which is believed to originate from a proximity to a Mott transition [1–8]. Whether an actual Mott insulator can be realized in the phase diagram of the iron pnictides remains an open question. In this work, we use transport, transmission electron microscopy (TEM), and neutron scattering experiments to demonstrate that Cu-doped $\text{NaFe}_{1-x}\text{Cu}_x\text{As}$ pnictides [9, 10] near $x \approx 0.5$ exhibit real space Fe and Cu ordering, and are antiferromagnetic (AF) insulators. In $\text{NaFe}_{1-x}\text{Cu}_x\text{As}$ with $x \approx 0.5$, the insulating behavior persists at temperatures above the Néel ordering temperature, thus indicating the presence of a Mott insulator phase. Based on studies of a multi-orbital Hubbard model within a slave-spin approach, we interpret this effect as arising from an effectively enhanced correlation strength associated with a Cu-site blockage of the kinetic motion of the Fe $3d$ electrons. Our discovery that a Mott insulating state can be induced near the iron pnictide superconductors highlights the important role of electron correlations in high-transition temperature (high- T_c) superconductivity.

At the heart of understanding the physics of the iron-based superconductors is the interplay among superconductivity, magnetism and bad-metal behavior [1–8]. Superconductivity occurs in the vicinity of antiferromagnetic order, both in the iron pnictides and iron chalcogenides [1–5]. In addition, superconductivity develops out of a normal state whose room-temperature resistivity is very large, reaching the Ioffe-Mott-Regel limit [2]. This bad-metal behavior has been attributed to the proximity to a Mott transition [6–8], with the Coulomb repulsion of the multi-orbital $3d$ electrons of the Fe ions being close to the threshold for electronic localization. In the iron chalcogenide family, several compounds have been found to be AF and insulating with characteristic features of a Mott insulator [11–14]. The issue, however, remains open in the iron pnictides.

Here we demonstrate that heavily Cu-doped $\text{NaFe}_{1-x}\text{Cu}_x\text{As}$ becomes an AF insulator when x approaches 0.5. Based on a slave-spin approach, we show that a Cu-site blockage of the kinetic motion of the Fe $3d$ electrons enhances the effect of electron correlations, pushing the system to the side of Mott localization. The parent compounds of iron pnictide superconductors such as $A\text{Fe}_2\text{As}_2$ ($A = \text{Ba}, \text{Sr}, \text{Ca}$) and NaFeAs have crystal structures shown in Fig. 1(a) and 1(b), respectively [2]. They exhibit a tetragonal to orthorhombic structural phase transition at temperature T_s , followed by a paramagnetic to AF phase transition at T_N ($T_s \geq T_N$) with a collinear magnetic structure where the spins are aligned antiferromagnetically along the a -axis of the orthorhombic lattice [Fig. 1(c)] [9]. When Fe in $A\text{Fe}_2\text{As}_2$ is replaced by Cu to form $ACu_2\text{As}_2$ [15], the Cu atoms have a nonmagnetic $3d^{10}$ electronic configuration with Cu^{1+} and a filled d shell due to the presence of a covalent bond between the As atoms within the same unit cell $[\text{As}]^{-3} \equiv [\text{As}-\text{As}]^{-4}/2$ shown in the shaded As-As bond of Fig. 1(a) [16–19], as predicted by band structure calculations [20]. Since the crystal structure of $\text{NaFe}_{1-x}\text{Cu}_x\text{As}$ does not allow a similar covalent bond [Fig. 1(b)] [10], it would be interesting to explore the magnetic state of $\text{NaFe}_{1-x}\text{Cu}_x\text{As}$ in the heavily Cu-doped regime. From transport measurements on single crystals of $\text{NaFe}_{1-x}\text{Cu}_x\text{As}$ with $x \leq 0.3$, it was found that the in-plane resistivity of the system becomes insulating-like for $x \geq 0.11$ [10].

We use transport and neutron scattering to study single crystals of $\text{NaFe}_{1-x}\text{Cu}_x\text{As}$ with $x = 0.016, 0.18, 0.39, 0.44, 0.48$ [Fig. 1(e) and 1(f)]. We have also carried out TEM measurements on the $x = 0.44$ sample [Fig. 2(a) and 2(b)]; sample characterization and experimental details are discussed in the Supplementary Information [21]. Instead of being a nonmagnetic sp metal as in the case of $ACu_2\text{As}_2$ [16–18], we have discovered that $\text{NaFe}_{1-x}\text{Cu}_x\text{As}$ near $x = 0.5$ becomes a charge and magnetically ordered insulator with a magnetic structure

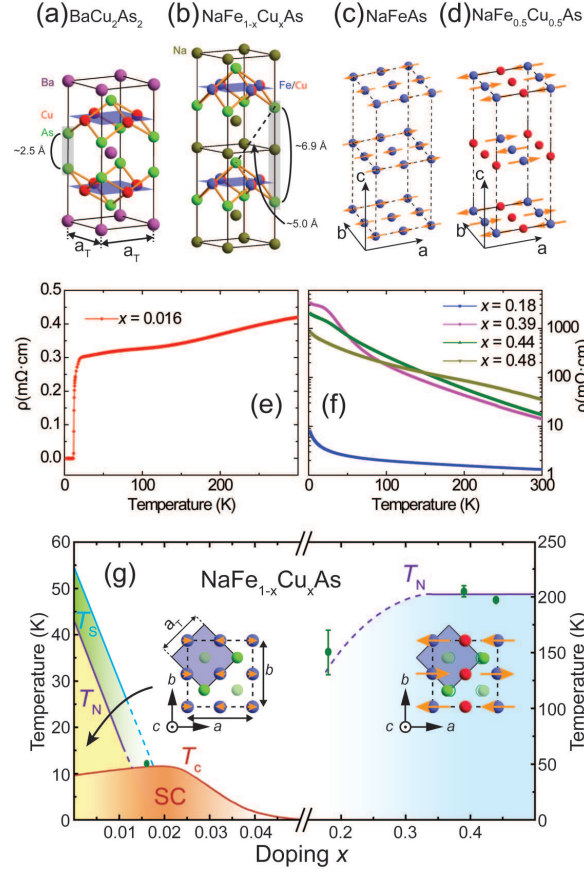


FIG. 1: **Summary of transport and neutron scattering results.** (a) The crystal structure of ACu_2As_2 in the tetragonal state, where a_T is the lattice parameter. The As-As covalent bonding distance is ~ 2.5 Å. (b) The crystal structure of $NaFe_{1-x}Cu_xAs$, where similar As-As covalent bonding is not possible. (c) The collinear magnetic structure of $NaFeAs$, where the AF order and moment direction are along the orthorhombic a axis [9]. Only Fe atoms are plotted in the figure for clarity. (d) Real space structure and spin arrangements of $NaFe_{0.5}Cu_{0.5}As$ in the AF orthorhombic unit cell similar to $NaFeAs$. In $NaFe_{0.5}Cu_{0.5}As$, since Fe and Cu form stripes, Na and As also shift slightly from their high symmetry positions. (e) In-plane resistivity for $x = 0.016$ sample where bulk superconductivity occurs below $T_c = 11$ K [10]. (f) Temperature dependence of the in-plane resistivity for $x = 0.18, 0.39, 0.44$, and 0.48 samples. (g) The electronic phase diagram of $NaFe_{1-x}Cu_xAs$ from resistivity and neutron scattering experiments. The left and right insets show the in-plane spin structure of $NaFeAs$ and the new AF insulating phase, respectively. For $x \leq 0.05$, the phase diagram is from ref. [10].

in Fig. 1(d). While undoped $NaFeAs$ has $T_s = 50$ K and $T_N = 39$ K with an ordered moment of $0.1 \mu_B/Fe$ [9], $NaFe_{0.56}Cu_{0.44}As$ orders antiferromagnetically below $T_N = 200$ K with a moment of $\sim 1.1 \mu_B/Fe$. The overall phase diagram of $NaFe_{1-x}Cu_xAs$ is shown in Fig. 1(g), where the left and right insets show the in-plane magnetic structures of $NaFeAs$ and $NaFe_{0.5}Cu_{0.5}As$, respectively.

To substantiate the key conclusions presented in Fig. 1, we prepared single crystals of $NaFe_{1-x}Cu_xAs$ with $x = 0.016, 0.18, 0.39, 0.44, 0.48$ using the flux method [21]. The Fe and Cu concentrations of the samples are determined from inductively coupled plasma (ICP) mass spectrometry analysis. Transport measurements were carried out using a commercial physical property measurement system (PPMS) with the standard four-probe method. Figure 1(e) shows temperature dependence of the in-plane resistivity for the $x = 0.016$ sample. In addition to superconductivity at $T_c = 11$ K, the normal state resistivity ρ is ~ 0.4 mΩ · cm at room temperature, consistent with previous work [10]. Figure 1(f) plots the temperature dependence of the resistivity on a log scale for $x = 0.18, 0.39, 0.44$, and 0.48 . Resistivity in the $x = 0.18$ sample is ~ 0.4 mΩ · cm, exhibiting insulating-like behavior consistent with earlier work [10]. For the $x \geq 0.39$ samples, resistivity further increase by an order of magnitude compared to the $x = 0.18$ sample, signifying electrons become much more localized in $NaFe_{1-x}Cu_xAs$ when x approaches 0.5.

Unpolarized and polarized elastic neutron scattering were carried out on $NaFe_{1-x}Cu_xAs$ single crystalline samples [21]. For these measurements, we use orthorhombic unit cell notation suitable for the AF ordered state of $NaFeAs$ [9], and define momentum transfer \mathbf{Q} in three-dimensional reciprocal space in Å^{-1} as $\mathbf{Q} = H\mathbf{a}^* + K\mathbf{b}^* + L\mathbf{c}^*$, where H ,

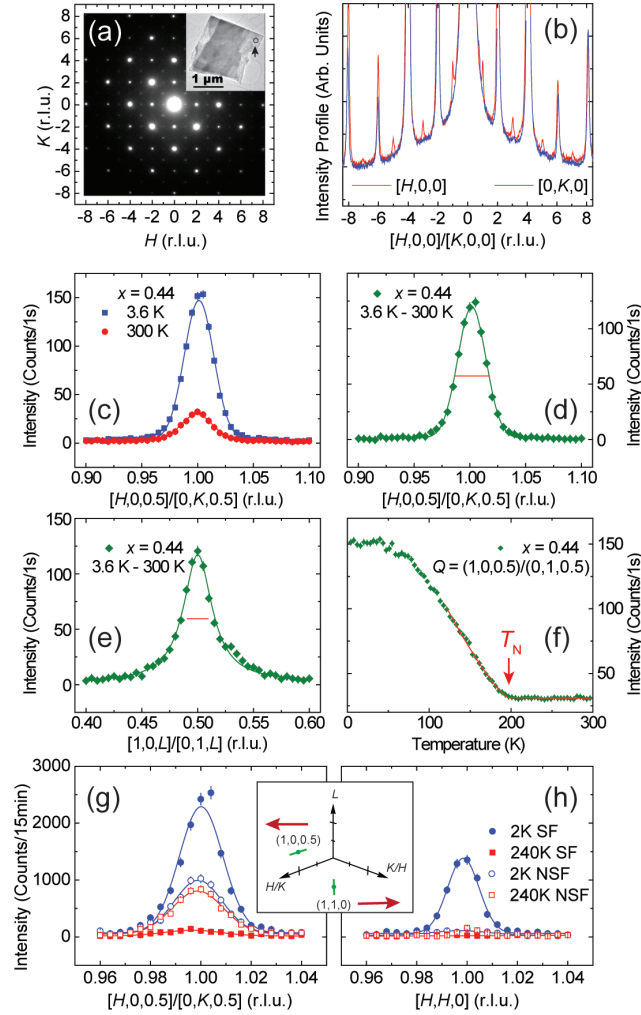


FIG. 2: **TEM, unpolarized and unpolarized neutron scattering results on the structure and magnetic order for $\text{NaFe}_{0.56}\text{Cu}_{0.44}\text{As}$.** (a) Using 200 keV incident electrons, an electron diffraction pattern along the $[H, K, 0]$ direction was obtained from a $\text{NaFe}_{0.56}\text{Cu}_{0.44}\text{As}$ particle with its TEM real-space image shown in the inset. (b) Cuts of Fig. (a) along the $[H, 0]$ and $[0, K]$ directions. (c) Unpolarized neutron diffraction scans along the $[H, 0, 0.5]/[0, K, 0.5]$ direction for the $x = 0.44$ sample at 300 K and 3.6 K. The peak at 300 K is a super-lattice peak arising from Fe-Cu ordering. Temperature difference plots between 3.6 K and 300 K along the (d) $[H, 0, 0.5]/[0, K, 0.5]$ and (e) $[1, 0, L]/[0, 1, L]$ directions. Solid lines are Gaussian fits and the horizontal bars indicate instrumental resolution. (f) Temperature dependence of the scattering at $\mathbf{Q} = (1, 0, 0.5)/(0, 1, 0.5)$ shows $T_N \approx 200$ K. (g) Neutron polarization analysis of the magnetic Bragg peak at $(1, 0, 0.5)/(0, 1, 0.5)$. Neutron SF and NSF cross sections are measured at 2 K and 240 K. The peak at 240 K is nonmagnetic nuclear scattering giving rise to NSF scattering. (h) Similar scans for the $(1, 1, 0)$ peak. The inset shows positions of these two peaks in reciprocal space.

K , and L are Miller indices and $\mathbf{a}^* = \hat{\mathbf{a}}2\pi/a$, $\mathbf{b}^* = \hat{\mathbf{b}}2\pi/b$, $\mathbf{c}^* = \hat{\mathbf{c}}2\pi/c$ [Fig. 1(c)]. Single crystals are aligned in the $(H, 0, L)$ and (H, H, L) scattering planes in the triple axis measurements. In the $(H, 0, L)$ scattering geometry, the collinear magnetic structure in NaFeAs [Fig. 1(c)] gives magnetic Bragg peaks below T_N at $\mathbf{Q}_{\text{AF}} = (H, 0, L)$, where $H = 1, 3, \dots$ and $L = 0.5, 1.5, \dots$, positions [9].

We begin by describing neutron scattering measurements on $\text{NaFe}_{0.56}\text{Cu}_{0.44}\text{As}$. Figure 2(c) shows typical elastic scans along the $[H, 0, 0.5]$ direction at $T = 3.6$ K and 300 K. Because of twinning in the orthorhombic state, this is equivalent to elastic scans along the $[0, K, 0.5]$ direction. While the scattering has a clear peak centered around $\mathbf{Q} = (1, 0, 0.5)/(0, 1, 0.5)$ at room temperature, the scattering is enhanced dramatically on cooling to 3.6 K, suggesting the presence of static AF order. The temperature difference plot between 3.6 K and 300 K in Fig. 2(d) indicates that the low-temperature intensity gain is essentially instrumentation resolution limited (horizontal bar). Figure 2(e) shows the temperature difference along the $[1, 0, L]/[0, 1, L]$ direction which apparently is not resolution limited. The temperature dependence of the scattering at $(1, 0, 0.5)/(0, 1, 0.5)$ plotted in Fig. 2(f) reveals clear evidence of magnetic

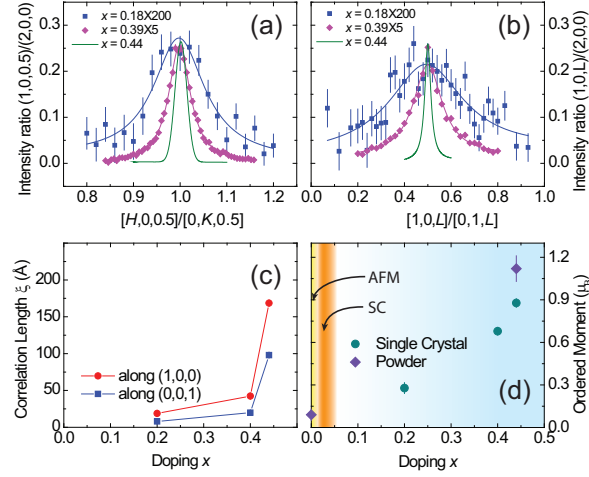


FIG. 3: **Cu-doping evolution of the structure and magnetic order for NaFe_{1-x}Cu_xAs.** (a) Comparison of the wave vector scans along the $[H, 0, 0.5]/[0, K, 0.5]$ direction for single crystals of $x = 0.18, 0.39,$ and 0.48 . The data are normalized to the $(2, 0, 0)$ nuclear Bragg peak. Note that intensity in the $x = 0.18$ and 0.39 samples are multiplied by 200 and 5 times, respectively. (b) Similar scans along the $[1, 0, L]/[0, 1, L]$ direction. (c) Cu-doping evolution of the spin-spin correlation length. (d) Cu-doping evolution of the ordered moment for the metallic AF, superconducting, and insulating AF phases of NaFe_{1-x}Cu_xAs.

ordering below $T_N \approx 200$ K, thus suggesting that the small peak at room temperature in Fig. 2(c) is a structural super-lattice peak induced by Cu substitution since it is forbidden for NaFeAs.

To conclusively determine the origin of super-lattice peaks and the crystal structure of NaFe_{0.56}Cu_{0.44}As, we have carried out high-resolution TEM measurements. The inset in Fig. 2(a) shows an image of the sample, and the electron diffraction patterns were collected from areas about 100 nm in diameter within a single domain of a twinned sample [see the arrow in the inset of Fig. 2(a)]. A typical diffraction pattern along the $[001]$ zone axis at room temperature is shown in Fig. 2(a). While we see clear super-lattice reflections at $H = 1, 3, \dots$ positions along the $[H, 0, 0]$ direction, they are absent at the $K = 1, 3, \dots$ positions along the $[0, K, 0]$ direction [Fig. 2(b)]. This means that the crystal structure of NaFe_{0.56}Cu_{0.44}As is orthorhombic and obeys two-fold rotational symmetry. From this information and intensities of super-lattice peaks in $(H, 0, L)$ scattering plane, we conclude that Fe and Cu in NaFe_{0.56}Cu_{0.44}As which NaFe_{0.56}Cu_{0.44}As approximates forms a real space stripe-like ordered structure in Fig. 1(d) with a space group *Ibam* [21]. The Fe-Cu ordering is a structural analogue of the magnetic order in NaFeAs and structural super-lattice peaks occur at the same positions as magnetic peaks in NaFeAs. Using this space group, we can refine the ordered magnetic moment using the crystal and magnetic structures in Fig. 1(d) [21].

Having established the real space Cu and Fe ordering and crystal structure of NaFe_{0.56}Cu_{0.44}As, it is important to determine the magnetic states of Cu and Fe. Assuming that the covalent As-As bonding is not possible because of the large distance between the neighboring As ions [see Fig. 1(b)], As ions in NaFe_{1-x}Cu_xAs can only be in the As³⁻ state. From X-ray absorption spectroscopy and preliminary Resonant Inelastic X-ray scattering experiments on NaFe_{0.56}Cu_{0.44}As that found no spin excitations at the Cu L_3 edge [21], we conclude that Cu in NaFe_{1-x}Cu_xAs is in the nonmagnetic Cu¹⁺ configuration. As a consequence, Fe must be in the Fe³⁺ $3d^5$ state since Na can only be in the Na¹⁺ state.

Assuming Fe in NaFe_{0.56}Cu_{0.44}As is indeed in the Fe³⁺ $3d^5$ state, we can determine the magnetic structure of the system by systematically measuring magnetic peaks at different wave vectors and using neutron polarization analysis. By polarizing neutrons along the direction of the momentum transfer \mathbf{Q} , neutron spin-flip (SF) scattering is sensitive to the magnetic components perpendicular to \mathbf{Q} and neutron non-spin-flip (NSF) scattering probes pure nuclear scattering [22, 23]. Figure 2(g) shows SF and NSF scans along the $[H, 0, 0.5]/[0, K, 0.5]$ direction at $T = 2$ K and 240 K. Inspection of the data reveals clear magnetic scattering at 2 K that disappears at 240 K, in addition to the temperature independent NSF nuclear super-lattice reflection. Figure 2(h) shows the SF and NSF scans along the $[H, H, 0]$ direction at 2 K and 240 K. While the SF scattering shows a clear peak at 2 K that disappears on warming to 240 K, the NSF scattering shows no evidence of the super-lattice peaks. From these results and systematic determination of magnetic and super-lattice scattering intensity at different wave vectors, we conclude that NaFe_{0.56}Cu_{0.44}As forms a magnetic structure with moments antiferromagnetically aligned along b axis but with the moments along the a axis direction as shown in the right inset in Fig. 1(g). The ordered magnetic moment is

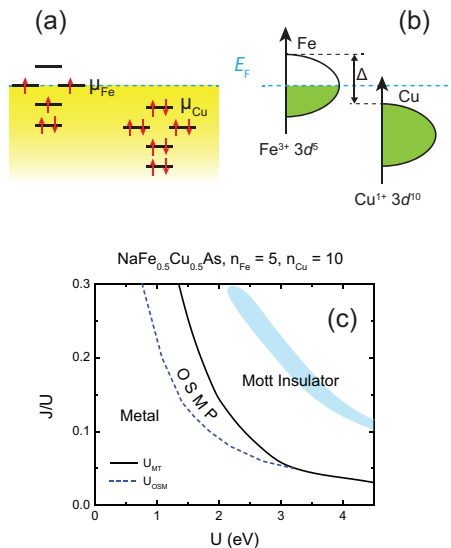


FIG. 4: **Summary of the schematic Cu and Fe electronic states and parameter regimes of a Mott insulator in the phase diagram.** Schematic of the electronic states of a Cu ion alongside those of an Fe ion, shown in terms of the atomic levels (a) and the electronic density of states (b). The relative potential difference associated with the two ions is specified in terms of an energy shift, Δ , as illustrated in (b). (c) The ground-state phase diagram of a multiorbital Hubbard model for NaFe $_{0.5}$ Cu $_{0.5}$ As. U_{OSM} and U_{MT} refer to the critical U values of an orbital-selective Mott (OSM) transition and a Mott transition (MT), respectively. The shaded region shows the *physical* parameter regime as determined by comparing the theoretically calculated bandwidth renormalization factors of the three t_{2g} orbitals with those determined by the ARPES results [21].

$1.12 \pm 0.09 \mu_B/\text{Fe}$ at 4 K [Fig. 3(d)] [21]. For this magnetic structure, magnetic peaks are expected at $(0, 1, 0.5)$ and $(1, 1, 0)$ positions which we have both observed Fig. 2(g)-(h). The magnetic peaks at $(0, 1, 0.5)$ overlap with super-lattice peaks at $(1, 0, 0.5)$ due to twinning.

To determine the Cu-doping dependence of the NaFe $_{1-x}$ Cu $_x$ As phase diagram, we carried out additional measurements on single crystals of NaFe $_{1-x}$ Cu $_x$ As with $x = 0.18$ and 0.39 [21]. Figures 3(a) and 3(b) compare the wave vector scans along the $[H, 0, 0.5]/[0, K, 0.5]$ and $[1, 0, L]/[0, 1, L]$ directions for $x = 0.18, 0.39$, and 0.44 . In each case, the scattering intensity is normalized to the $(2, 0, 0)$ nuclear Bragg peak. With increasing Cu-doping, the scattering profile becomes narrower and stronger, changing from a broad peak indicative of the short-range magnetic order in $x = 0.18, 0.39$ to an essentially instrument resolution limited peak with long-range magnetic order at $x = 0.44$. Figure 3(c) shows the doping evolution of the spin-spin correlation length ξ in NaFe $_{1-x}$ Cu $_x$ As, suggesting that the increasing spin correlations in NaFe $_{1-x}$ Cu $_x$ As are related to the increasing Cu-doping. The Cu-doping dependence of the ordered moment, determined from single crystal and powder neutron diffraction measurements, are shown 3(d). In the undoped state, NaFeAs has an ordered moment of $\sim 0.1 \mu_B/\text{Fe}$ [9]. Upon Cu-doping to induce superconductivity at $x = 0.02$, the static AF order is suppressed [10]. With further Cu doping, the system becomes an AF insulator, where the ordered moment reaches $\sim 1.1 \mu_B/\text{Fe}$ at $x = 0.44$. The ordered moment is determined for per Fe site in the structure for NaFe $_{0.5}$ Cu $_{0.5}$ As [Fig. 1(d)]. Since the iron moment in NaFe $_{1-x}$ Cu $_x$ As increases with increasing Cu-doping, our determined moment is therefore a lower bound for the ordered moment for Fe in the ideal NaFe $_{0.5}$ Cu $_{0.5}$ As which can have either $S = 3/2$ or $S = 5/2$.

The behavior in NaFe $_{1-x}$ Cu $_x$ As is entirely different from the bipartite magnetic parent phases seen in the iron oxypnictide superconductor LaFeAsO $_{1-x}$ H $_x$, where magnetic parent phases on both sides of the superconducting dome are metallic antiferromagnets [24]. In Cu-doped Fe $_{1-x}$ Cu $_x$ Se, a metal-insulator transition has been observed around 4% Cu-doping, and a localized moment with spin glass behavior is found near $x \approx 0.12$ [25, 26]. Although the density functional theory (DFT) calculations suggest that Cu occurs in the $3d^{10}$ configuration and the metal-insulator transition is due to disorder induced Anderson localization in Fe $_{1-x}$ Cu $_x$ Se [27], the 20-30% solubility limit of the system [25] means it is unclear if Fe $_{1-x}$ Cu $_x$ Se is also an AF insulator at $x \approx 0.5$.

It is useful to compare our experimental findings with the results of the band structure calculations based on the density function theory (DFT). Both the DFT and DFT+ U calculations clearly predict the paramagnetic phase of NaFe $_{0.5}$ Cu $_{0.5}$ As to be a metal [21]. By contrast, our measurements have shown that the insulating behavior of the resistivity persists above the Néel temperature [Fig. 1(f)], implying that NaFe $_{0.5}$ Cu $_{0.5}$ As is a Mott insulator.

To understand the origin of the Mott insulating behavior, we address how Cu-doping affects the effect of electron correlations. Our starting point is that the local (ionization) potential difference between the Fe and Cu ions, as illustrated in Fig. 4(a) and described by the energy shift Δ in Fig. 4(b), will suppress the hopping integral between Fe and Cu sites. This causes a reduction in the kinetic energy or, equivalently, the electron bandwidth. The ratio of the on-site Coulomb repulsion U (including the Hund's coupling J_H) relative to the bandwidth will effectively increase, even if the raw values of U and J_H remain the same as in pure NaFeAs. This would enhance the tendency of electron localization even without considering the disorder effects with increasing x [28, 29].

The case of $x = 0.5$ allows a detailed theoretical analysis. Here, the Cu and Fe ions in NaFe_{1-x}Cu_xAs have real space ordering, as discussed before. We study the metal-insulator transition in multi-orbital Hubbard models for NaFe_{0.5}Cu_{0.5}As via the $U(1)$ slave-spin mean-field theory [30]. We use the tight-binding parameters for NaFeAs, and consider the limit of a large local potential difference between Cu and Fe, which transfers charge from Fe to Cu to Cu¹⁺ ($n = 10$). The fully occupied Cu $3d$ shell makes the Cu ions essentially as vacancies. The reduction of the Fe $3d$ electron bandwidth caused by this kinetic blocking effect is demonstrated in the Supp. Info [Fig. S10]. The resulting ground state phase diagram is shown in Fig. 4(c). For realistic parameters, illustrated by the shaded region, a Mott localization takes place.

Our work uncovers a Mott insulator, NaFe_{0.5}Cu_{0.5}As, right in the middle of the phase diagram of a superconducting iron pnictide. Our discovery provides evidence that the electron correlations of the iron pnictides, while weaker than those of the iron chalcogenides, are sufficiently strong to place these materials in close proximity to Mott localization [31]. This finding makes it natural that the electron correlation and the associated bad-metal behavior and magnetism induce a similarly high superconducting transition temperature in the iron pnictides and chalcogenides. Such a commonality, in spite of the very different chemical composition and electronic structure of the two broad classes of materials, introduces considerable simplicity in the quest for a unified framework of the iron-based superconductivity. More generally, the proximity to Mott transition links the superconductivity of the iron pnictides to that arising in the copper oxides and organic charge-transfer salts [32], and suggest that the same framework applies to all these strongly correlated electronic systems.

-
- [1] Y. Kamihara, T. Watanabe, M. Hirano, and H. Hosono, *Iron-based layered superconductor* La[O_{1-x}F_x]FeAs ($x = 0.05-0.12$) with $T_c = 26$ K, *J. Am. Chem. Soc.* **130**, 3296-3297 (2008).
- [2] G. R. Stewart, *Superconductivity in iron compounds*, *Rev. Mod. Phys.* **83**, 1589-1652 (2011).
- [3] Clarina de la Cruz, Q. Huang, J. W. Lynn, Jiying Li, W. Ratcliff II, J. L. Zarestky, H. A. Mook, G. F. Chen, J. L. Luo, N. L. Wang & Pengcheng Dai, *Magnetic order close to superconductivity in the iron-based layered LaO_{1-x}F_xFeAs systems*, *Nature* **453**, 899-902 (2008).
- [4] P. C. Dai, J. P. Hu, and E. Dagotto, *Magnetism and its microscopic origin in iron-based high-temperature superconductors*, *Nat. Phys.* **8**, 709 (2012).
- [5] D. J. Scalapino, *A common thread: the pairing interaction for the unconventional superconductors*, *Rev. Mod. Phys.* **84**, 1383 (2012).
- [6] Q. Si & E. Abrahams, *Strong correlations and magnetic frustration in the high T_c iron pnictides*, *Phys. Rev. Lett.* **101**, 076401 (2008).
- [7] M. M. Qazilbash, J. J. Hamlin, R. E. Baumbach, Lijun Zhang, D. J. Singh, M. B. Maple & D. N. Basov, *Electronic correlations in the iron pnictides*, *Nat. Phys.* **5**, 647 (2009).
- [8] Z. P. Yin, K. Haule, & G. Kotliar, *Kinetic frustration and the nature of the magnetic and paramagnetic states in iron pnictides and iron chalcogenides*, *Nature Materials* **10**, 932-935 (2011)
- [9] Shiliang Li, Clarina de la Cruz, Q. Huang, G. F. Chen, T.-L. Xia, J. L. Luo, N. L. Wang, and Pengcheng Dai, *Structural and magnetic phase transitions in Na_{1-δ}FeAs*, *Phys. Rev. B* **80**, 020504(R) (2009).
- [10] A. F. Wang, J. J. Lin, P. Cheng, G. J. Ye, F. Chen, J. Q. Ma, X. F. Lu, B. Lei, X. G. Luo, and X. H. Chen, *Phase diagram and physical properties of NaFe_{1-x}Cu_xAs single crystals*, *Phys. Rev. B* **88**, 094516 (2013).
- [11] J.-X. Zhu, R. Yu, H. D. Wang, L. L. Zhao, M. D. Jones, J. H. Dai, E. Abrahams, M. H. Fang, and Q. Si, *Band narrowing and Mott localization in iron oxychalcogenides La₂O₂Fe₂O(Se,S)*, *Phys. Rev. Lett.* **104**, 216405 (2010).
- [12] M. H. Fang, H. D. Wang, C. H. Dong, Z. J. Li, C. M. Feng, J. Chen, and H. Q. Yuan, *Fe-based superconductivity with $T_c = 31$ K bordering an antiferromagnetic insulator in (Tl,K)Fe_xSe₂*, *EPL* **94**, 27009 (2011).
- [13] T. Katasea, H. Hiramatsu, T. Kamiya, and H. Hosono, *Electric double-layer transistor using layered iron selenide Mott insulator TlFe_{1.6}Se₂*, *PNAS* **111**, 3979-3983 (2014).
- [14] T. K. Chen *et al*, *Fe-vacancy order and superconductivity in tetragonal β -Fe_{1-x}Se*, *PNAS* **111**, 63-68 (2014).
- [15] M. Pfisterer & G. Nagorsen, *On the structure of ternary arsenides*, *Z. Naturforsch. B* **35B**, 703-704 (1980).
- [16] V. K. Anand, P. Kanchana Perera, Abhishek Pandey, R. J. Goetsch, A. Kreyssig, and D. C. Johnston, *Crystal growth and physical properties of SrCu₂As₂, SrCu₂Sb₂, and BaCu₂Sb₂*, *Phys. Rev. B* **85**, 214523 (2012).
- [17] Y. J. Yan, P. Cheng, J. J. Ying, X. G. Luo, F. Chen, H. Y. Zou, A. F. Wang, G. J. Ye, Z. J. Xiang, J. Q. Ma, and X. H.

- Chen, *Structural, magnetic, and electronic transport properties of hole-doped SrFe_{2-x}Cu_xAs₂ single crystals*, Phys. Rev. B **87**, 075105 (2013).
- [18] J. A. McLeod, E. Z. Kurmaev, I. Perez, V. K. Anand, P. Kanchana Perera, D. C. Johnston, and A. Moewes, *Electronic structure of copper pnictides: Influence of different cations and pnictogens*, Phys. Rev. B **88**, 014508 (2013).
- [19] Hikaru Takeda, Takashi Imai, Makoto Tachibana, Jonathan Gaudet, Bruce D. Gaulin, Bayrammurad I. Saporov, and Athena S. Sefat, *Cu substitution effects on the local magnetic properties of Ba(Fe_{1-x}Cu_x)₂As₂: a site-selective ⁷⁵As and ⁶³Cu NMR study*, Phys. Rev. Lett. **113**, 117001 (2014).
- [20] D. J. Singh, *Electronic structure of BaCu₂As₂ and SrCu₂As₂: sp-band metals*, Phys. Rev. B **79**, 153102 (2009).
- [21] Materials and methods are available as supplementary information online.
- [22] Yu Song, Louis-Pierre Regnault, Chenglin Zhang, Guotai Tan, Scott V. Carr, Songxue Chi, A. D. Christianson, Tao Xiang, and Pengcheng Dai, *In-plane spin excitation anisotropy in the paramagnetic state of NaFeAs*, Phys. Rev. B **88**, 134512 (2013).
- [23] R. M. Moon, T. Riste, & W. C. Koehler, *Polarization Analysis of Thermal-Neutron Scattering*, Phys. Rev. **181**, 920-931 (1969).
- [24] M. Hiraishi, S. Iimura, K. M. Kojima, J. Yamaura, H. Hiraka, K. Ikeda, P. Miao, Y. Ishikawa, S. Torii, M. Miyazaki, I. Yamauchi, A. Koda, K. Ishii, M. Yoshida, J. Mizuki, R. Kadono, R. Kumai, T. Kamiyama, T. Otomo, Y. Murakami, S. Matsuishi & H. Hosono, *Bipartite magnetic parent phases in the iron oxy pnictide superconductor*, Nat. Phys. **10**, 300-303 (2014).
- [25] A. J. Williams, T. M. McQueen, V. Ksenofontov, C. Felser & R. J. Cava, *The metal-insulator transition in Fe_{1.01-x}Cu_xSe*, J. Phys. Condens. Matter **21**, 305701 (2009).
- [26] Tzu-Wen Huang, Ta-Kun Chen, Kuo-Wei Yeh, Chung-Ting Ke, Chi Liang Chen, Yi-Lin Huang, Fong-Chi Hsu, Maw-Kuen Wu, Phillip M. Wu, Maxim Avdeev, and Andrew J. Studer, *Doping-driven structural phase transition and loss of superconductivity in M_xFe_{1-x}Se_δ (M = Mn, Cu)*, Phys. Rev. B **82**, 104502 (2010).
- [27] Stanislav Chadov, Daniel Schrf, Gerhard H. Fecher, Claudia Felser, Lijun Zhang, and David J. Singh, *Electronic structure, localization, and spin-state transition in Cu-substituted FeSe:Fe_{1-x}Cu_xSe*, Phys. Rev. B **81**, 104523 (2010).
- [28] H. Wadati, I. Elfimov, & G. A. Sawatzky, *Where Are the Extra d Electrons in Transition-Metal Substituted Fe Pnictides?*, Phys. Rev. Lett **105**, 157004 (2010).
- [29] T. Berlijn, C. -H. Lin, W. Garber, & W. Ku, *Do Transition Metal Substitutions Dope Carriers in Iron Based Superconductors?*, Phys. Rev. Lett. **108**, 207003 (2012).
- [30] R. Yu, & Q. Si, *U(1) Slave-spin theory and its application to Mott transition in a multi-orbital model for iron pnictides*, Phys. Rev. B **86**, 085104 (2012).
- [31] R. Yu, P. Goswami, Q. Si, P. Nikolic, & J.-X. Zhu, *Superconductivity at the Border of Electron Localization and Itinerancy*, Nat. Commun. **4**, 2783 (2013).
- [32] P. A. Lee, N. Nagaosa, & X. G. Wen, *Doping a Mott insulator: Physics of high-temperature superconductivity*, Rev. Mod. Phys. **78**, 17-85 (2006).

Acknowledgments We thank X. H. Chen and Lijun Wu for helpful discussions, Leland Harriger, Scott Carr, Weiyi Wang, and Binod K. Rai for assisting with some experiments. The single crystal growth and neutron scattering work at Rice is supported by the U.S. DOE, BES under contract no. de-sc0012311 (P.D.). The theoretical work at Rice was in part supported by the Robert A. Welch Foundation Grant No. C-1818 (A.H.N.), C-1411 (Q.S), by U.S. NSF grants DMR-1350237 (A.H.N.) and DMR-1309531 (Q.S.), and by the Alexander von Humboldt Foundation (Q.S.). E.M. and J.C. acknowledge support from the DOD PECASE. The electron microscopy study at Brookhaven National Laboratory was supported by the U.S. DOE, BES, by the Materials Sciences and Engineering Division under Contract No. DE-AC02-98CH10886. The use of ORNL's High Flux Isotope Reactor was sponsored by the Scientific User Facilities Division, Office of BES, U.S. DOE.

Author contributions

Most of the single crystal growth and neutron scattering experiments were carried out by Y.S. with assistance from Y.L., C.Z., Q.H., H.W., W.T., and S.C. The polarized neutron scattering experiments were performed by Z.Y. TEM measurements were carried out by J.T. and Y.M.Z. Transport and ICP measurements were carried out by C.C., J.C., under the supervision of E.M. The theoretical work was done by R.Y., A.H.N, and Q.S. P.D. provided the overall lead of the project. The paper was written by P.D., Y.S., A.H.N., R.Y., and Q.S. All authors provided comments.

Additional information The authors declare no competing financial interests.

Correspondence and requests for materials should be addressed to Q.S. (qmsi@rice.edu) or P.D. (e-mail: pdai@rice.edu)